

## Structural incoherency and structure reversal in bimetallic Au-Pd nanoclusters

H. B. Liu,<sup>1</sup> U. Pal,<sup>2,\*</sup> A. Medina,<sup>3</sup> C. Maldonado,<sup>3</sup> and J. A. Ascencio<sup>1</sup>

<sup>1</sup>Programa de Investigación y Desarrollo de Ductos, Instituto Mexicano del Petroleo, Eje Central Lázaro Cárdenas No. 152, Col. San Bartolo Atepehuacan, C.P.07730, Mexico D.F., Mexico

<sup>2</sup>Instituto de Física, Universidad Autónoma de Puebla, Apdo. Postal J-48, Puebla, Pue. 72570, Mexico

<sup>3</sup>Instituto de Investigaciones Metalúrgicas, UMSNH, Edificio U. Ciudad Universitaria, Morelia, Michoacán, 58000, Mexico  
(Received 26 April 2004; revised manuscript received 14 July 2004; published 3 February 2005)

Colloidal bimetallic nanoclusters of Au-Pd were synthesized by simultaneous reduction of the metal ions from their corresponding chloride salts with polymer (PVP) stabilizer. Structural characterization of the samples with different Au/Pd ratios was made using high-resolution electron microscopy. Classical molecular dynamics simulation is used for structural thermodynamics and dynamic analysis of the bimetallic clusters. Structural incoherency and structure reversal mechanism in such bimetallic clusters were studied systematically for different atomic configurations, which explain the anomalies on the reported experimental results on such nanoclusters mainly by electron microscopy. Our simulation and experimental results revealed that stable ordered structures of the bimetallic cluster are Pd core/Au shell, random solid solutions and eutecticlike configurations. Though the Au-core/Pd-shell structure is stable at low temperature, the structure changes to Pd core/Au shell on heating at about 500 K.

DOI: 10.1103/PhysRevB.71.075403

PACS number(s): 61.46.+w, 82.20.Wt, 36.40.Sx, 36.40.Ei

### I. INTRODUCTION

Au-Pd bimetallic nanoclusters are the most attractive catalyst for the direct synthesis of hydrogen peroxide from H<sub>2</sub> and O<sub>2</sub>,<sup>1</sup> hydrodesulfurization of thiophene,<sup>2</sup> and other catalytic applications.<sup>3,4</sup> Recently, the technique for their nanocontact applications<sup>5</sup> has been developed. The catalytic performance of Au-Pd bimetallic nanoclusters is benefited to a great extent from their structural diversities, such as alloy cluster,<sup>6–13</sup> wire,<sup>14</sup> lithographic patterns,<sup>15</sup> and core-shell<sup>16–18</sup> clusters. According to the phase diagram, Au-Pd is likely to form solid solutions of arbitrary compositions at low temperatures.<sup>19</sup> Dilute-limit heat of solution in the cases of Au in Pd host is about  $-0.33$  eV and Pd in Au host is about  $-0.29$  eV,<sup>20</sup> which are the right values for the bimetallics to form a variety of structures. In fact, it has been found that the Au-Pd bimetallic nanoclusters often have so-called core-shell structures if they are prepared by alcohol reduction of Au and Pd ions in the presence of a water-soluble polymer-like poly(*N*-vinyl-2-pyrrolidone) (PVP), and that the core-shell structured bimetallic nanoclusters have much higher catalytic activity than the corresponding monometallic nanoclusters. Though the Pd-core/Au-shell structure is usually expected, the synthesis of the Au-core/Pd-shell structure is also reported.<sup>18</sup> Composition and atom distribution in the alloy clusters strongly depend on the synthesis methods<sup>9,17</sup> and probably also on process variables. Probably these are the reasons why we encounter several contradictory reports on the structure of bimetallic nanoclusters prepared by similar techniques and of similar composition. To make a clarification of the above mentioned confusions, we performed the structural analysis of several Au-Pd nanoclusters with different compositions both experimentally and theoretically to reveal the thermodynamics and dynamic structural behavior of Au-Pd nanoclusters. Our analysis predicts and demonstrates that depending on the composition and process parameters, the nanoclusters of several structures can coexist even for the

samples prepared by a single technique. Conditions for the coexistence and structural transformation of such nanoclusters are determined.

### II. RESEARCH METHODS

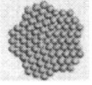
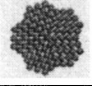
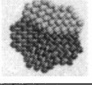
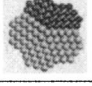
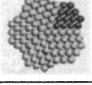
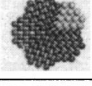
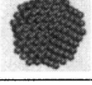
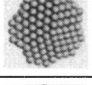
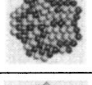
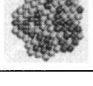
#### A. Experiment

The synthesis of bimetallic Au-Pd colloidal particles was performed by simultaneous reduction of corresponding metal chloride salts in the presence of PVP, as reported in detail elsewhere.<sup>21</sup> Structural characterization of the samples was made using a Schottky field emission JEOL JEM2010-F microscope with analytical equipments attached. The samples for microscopic observations were prepared by spreading a drop of colloidal solution onto a carbon film supported by a Cu grid and subsequent drying in vacuum. The samples were analyzed by high-resolution electron microscopy (HREM). The HREM images were processed digitally in the real and Fourier spaces.

#### B. Simulation

For the molecular dynamics (MD) simulation, interatomic interactions between Au and Pd were described by a simple analytical embedded-atom method (EAM) developed by Cai and Ye.<sup>22</sup> The model includes a long-range force. In this model, the electron-density function is taken as a decreasing exponential function; the two-body potential is defined as a function given by Rose *et al.*,<sup>25</sup> and the embedding energy is assumed to be a universal form suggested by Banerjee and Smith.<sup>23</sup> The alloy model of Johnson<sup>24</sup> is applied and an extra parameter is introduced in order to fit dilute-limit heats of solution. For the three possible compositions treated in this work (Au<sub>1</sub>Pd<sub>5</sub>, Au<sub>1</sub>Pd<sub>1</sub>, and Au<sub>5</sub>Pd<sub>1</sub>), the predicted heats of formation are in reasonable agreement with first-principles calculations and experimental data, and consistent lattice

TABLE I. The formation energy of Au-Pd bimetal decahedral clusters with 262 atoms at 298 K.

Morphology	Type of structure	component	Total cohesive energy, eV	Stoichiometry energy, eV ( $c_{Au}E_{Au}+c_{Pd}E_{Pd}$ )	Total formation energy of bimetal, eV
	Pure Au	262 Au 0 Pd	-999.16425	-999.1632	0
	Pure Pd	0 Au 262 Pd	-973.76964	-973.77016	0
	Eutectic-like	84 Au 178 Pd	-977.40358	-981.91144	4.50786
	Eutectic-like	178 Au 84 Pd	-982.38289	-991.02192	8.63903
	Eutectic-like	229 Au 33 Pd	-995.18159	-995.96484	0.78325
	Eutectic-like	33 Au 229 Pd	-977.12586	-976.96852	-0.15734
	Au-Core/Pd-shell	99 Au 163 Pd	-964.21869	-983.36524	19.14655
	Pd-Core/Au-shell	163 Au 99 Pd	-1004.47368	-989.56812	-14.90556
	Solid solution	131 Au 131 Pd	-990.66811	-986.46668	-4.20143
	Solid solution	163 Au 99 Pd	-990.32411	-989.56812	-0.75599

constants are predicted. The Au-Pd alloying potential can be used for a wide range of components with great accuracy. The MD simulations were performed using the program XMD developed by Riffkin.<sup>26</sup> The program employs a predictor-corrector algorithm to integrate the equation of motion. A time step of  $5 \times 10^{-15}$  s (5 fs) was used. Each configuration was fully relaxed by a long process of  $4 \times 10^6$  time steps, about  $2 \times 10^{-8}$  s each.

### III. RESULTS AND DISCUSSION

In order to determine the morphology and the mode of formation of Au-Pd bimetallic clusters, 262-atom decahedra and 861-atom cuboctahedron with different compositions and distributions were built from the classic molecular dynamics simulation (see the images in Table I). These structures include eutectic-like and core-shell-like configurations along with random solid solutions. To determine the possibility of formation of each of the structures, the total cohesive energy, stoichiometric energy, and the corresponding formation energies are evaluated and presented in Table I.

Our results revealed that the Pd-core/Au-shell bimetallic structures have the lowest heat of formation. Random solid solutions have a negative heat of alloy formation with smaller absolute values. However, they have much higher entropy in comparison with core-shell and eutectic structures. Therefore, the Gibbs free energy in random solid solutions may be a bit more negative. Eutecticlike structures are favorable when the alloy is rich in either of its constituents. As there exists a lot of isomers for the one-component enriched structures, it is difficult to predict the most favorable structure among them. Our results demonstrate at least that the structures enriched with either of the components is also favorable energetically. In general, the differences in energies among the configurations are relatively low and the coexistence of these structures must be the common feature in the samples synthesized by any technique. As the critical number of atoms are needed to produce each type of nanoclusters, the formation of both decahedrons and octahedrons are probable in the synthesized sample and the synthesis conditions determine the kind of configuration of the clusters based on their surface energy reduction capacity.

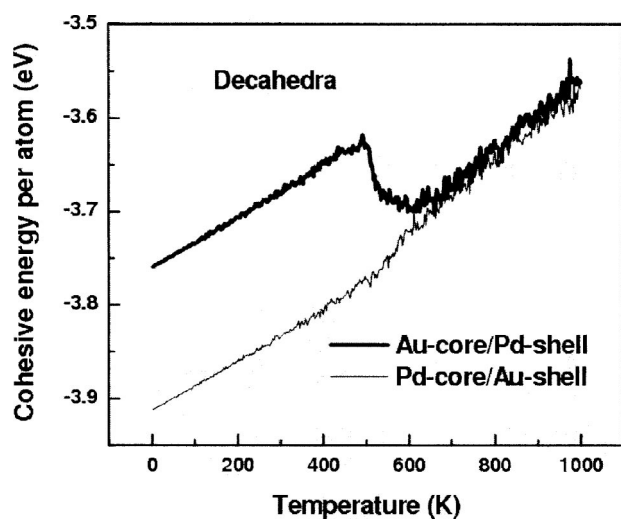


FIG. 1. Variation of cohesive energy per atom with temperature.

For the embedding-atom model, the alloying pair potential determines the magnitude of chemical order. In the Cai-Ye model,<sup>22</sup> the Au-Pd alloying pair potential is very close to the mathematical average of Au-Au and Pd-Pd pair potentials, which indicates that the bimetal formation potential is very small and it must not affect the bimetal formation energy significantly. The other factor affecting bimetal formation is the incoherency of the structure, which may dominate the process of bimetallic aggregation and configuration. There exists structural incoherency for all the structures treated here, while the core-shell structures of Au covering Pd has the minimum incoherency. This effect is attributed to the contraction of the Au surface, leading to a good accommodation with the Pd core, which has a smaller nearest-neighbor distance, hence producing a small structural mismatch for the Pd core. For the core shell with Pd covering Au, the Au core has a maximum structure incoherent energy. In general, structural incoherency dominates the formation process of Au-Pd bimetal clusters, and the core-shell structure with Au covering Pd is energetically favorable.

In order to determine the stability condition of the unstable Au-core/Pd-shell bimetallic nanoclusters, we carried out heating processes from 0 K to 1000 K. The temperature was increased linearly by heating at the rate of  $5 \times 10^{10}$  K/s for a total duration of  $2 \times 10^{-8}$  s. As a result, the cohesive energies at different temperatures were determined for the decahedral Au-core/Pd-shell and Pd-core/Au-shell structures (Fig. 1). It can be seen that the cohesive energy of the unstable Au-core/Pd-shell bimetallic nanocluster dropped suddenly at about 500 K, and then approached the values of its reverse structure (Pd-core/Au-shell) at temperatures higher than 620 K.

Through the observation on the trajectories of the above processes, it can be found that the sudden drop in cohesive energy for Au-core/Pd-shell structure is induced by the position reversal of the shell and core atoms, i.e., the Pd atoms of the shell enter into the core and finally are covered by Au atoms. This result supports the dynamical point of view of our conclusion that Au-core/Pd-shell structures are not stable

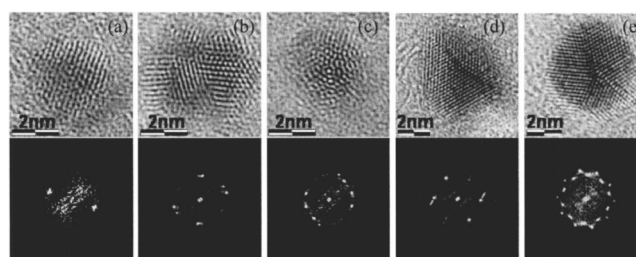


FIG. 2. HREM images of different representative structures revealed in the  $\text{Au}_1\text{Pd}_1$  sample along with their corresponding FFT's.

and cannot exist beyond a certain temperature. In practice, Au-core/Pd-shell structures, which have a good selectivity in catalytic reactions,<sup>27</sup> can be synthesized and should be used at low temperatures. Moreover, during the reversal of core/shell structure, the decahedron loses its morphology and changes to a rounded disordered structure. The change in slope of the cohesive energy versus temperature curve beyond 500 K is due to melting. It is found that the core-shell configurations persist even at 1000 K.

A similar observation has been made for 861-atom cuboctahedron; therefore, the details of the results are not included here.

Experimental studies were performed on the Au-Pd nanoclusters with different nominal compositions (Au/Pd molar ratios 1/1, 5/1, and 1/5) through low magnification transmission electron microscope (TEM) and HREM images to evaluate the size distribution and internal structure of the produced nanoparticles, respectively. Our experimental results indicate that the composition of nanoparticles plays an important role on their structure. In the case of monometallic Au and Pd particles, the observed structures for smallest clusters around 1–5 nm are quite similar, based on the fcc symmetry for bulk crystals but with multiple twins (mtp).

In Fig. 2 we present a representative collection of the observed configurations for the  $\text{Au}_1\text{Pd}_1$  clusters. In our previous work we reported a simple way to determine the structure of small nanoparticles using HREM images,<sup>28</sup> where we established the structure and orientation for each observed HREM. The image shown in the Fig. 2(a) corresponds to a 3.4-nm-size fcc-like cluster, where the contrast is based on equidistance parallel lines, even when a small deformation can be observed at the center of the particle. The corresponding fast Fourier transform (FFT) shows just one reflection but with a clear deformation of the dot, increasing its length and width representing small deformations in the lattice both in orientation and distance. From the HREM image and its FFT we could determine an orientation close to  $\{125\}$  with respect to the electron beam. In the case of the particle with diameter of 5.7 nm shown in Fig. 2(b), an interesting contrast is recognized where three main domains could be identified: one kind of fringe in two orientations (at the left and at the center), and well-defined hexagons at the right boundary. Its corresponding FFT shows the effect of the arrays with an hexagon associated to a fcc-like cluster in the  $\{011\}$  orientation including extra points of different intensities, a common feature of twin structures. A small elongation to the internal region (in the FFT) demonstrates the formation of bimetallic

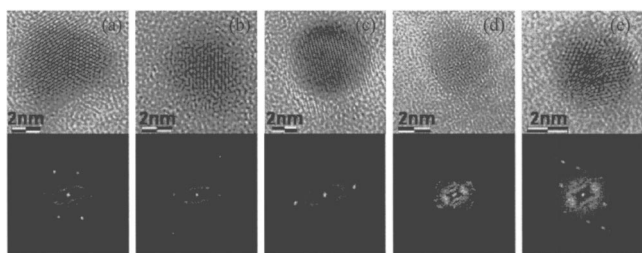


FIG. 3. HREM analysis of small nanoparticles observed for  $Au_5Pd_1$ . The HREM are shown with their corresponding FFT's.

structure. In Fig. 2(c), an icosahedral particle of 2.4 nm size is identified with characteristic onionlike contrast and multiple points in the FFT with near fivefold orientation. A single twin particle of 5.2 nm at the  $\{011\}$  is identified in Fig. 2(d), even though the contrast is not simple to be recognized. In the corresponding FFT, the clear presence of an extra elongated dot denotes the twin in the particle. Finally, several well-defined decahedral particles could be found in the sample. In Fig. 2(e) a decahedral particle of 5.4 nm size with fivefold orientation is shown with its classical FFT.

In the case of high concentration of Au ( $Au_5Pd_1$ ), the shape and structure of the particles tend to be more defined by the bulk lattice and a high concentration of fcc-like clusters could be found. In Fig. 3(a), a pyramid shaped particle of 5 nm size with hexagonal dot array is shown. Its FFT denotes the perfect hexagonal array of the atoms with fcc-like structure in the  $\{111\}$  orientation. Two particles of 5 and 7 nm sizes with rounded profiles and parallel internal fringe contrasts are shown in Figs. 3(b) and 3(c), respectively. These contrasts are common in fcc-like particles and their FFT reveal an orientation close to  $\{125\}$ . Beside these nice fcc-like ordered clusters, a few disordered clusters could be identified [Fig. 3(d)] with multiple defects, producing highly distorted images and multiple dots in their FFT, while in Fig. 3(e), a cluster with core-shell contrast could be observed. In its FFT, it is possible to distinguish extra dots away from the hexagonal array of a fcc-like structure in  $\{011\}$  orientation. The external dots are produced by closely spaced lines in the core of the cluster, indicating probably the presence of the Pd

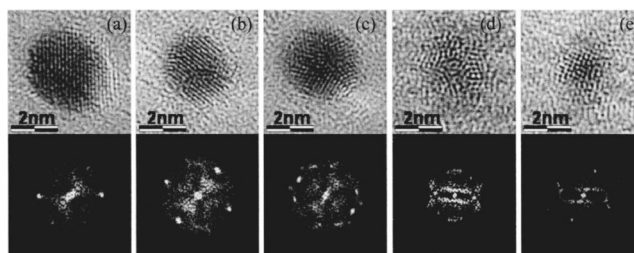


FIG. 4. HREM images of different representative structures revealed in the  $Au_1Pd_5$  sample with corresponding FFT's.

core inside the Au shell. We have also seen a few Au-core/Pd-shell structures in this sample and the  $Au_1Pd_5$  sample.

Finally the case of particles produced with an extra Pd concentration ( $Au_1Pd_5$ ) is presented in Fig. 4. In this case, the clusters are smaller and have more twins and defects than in the previous cases. However, it is clear that they are also related to the fcc-like structures [Fig. 4(a)] having rounded shapes and parallel line contrasts with  $\{125\}$  orientation. In the Fig. 4(b), we can identify a small deformation in a particle of 2.3 nm size, producing a square contrast FFT which corresponds to a perpendicular defect seen clearly at the center of the particle. A decahedron with fivefold orientation can be identified from the image of Fig. 4(c). A 2.6-nm mtp with truncated icosahedron contrast at  $\{122\}$  orientation is shown in Fig. 4(d). Finally, in Fig. 4(e), a really small particle of about 1.6 nm diameter, having a truncated octahedron contrast with  $\{001\}$  orientation, is shown. While the small structural deformations are usual for such the small clusters, the observed elongated symmetry in the FFT is due to a small rotation of the particle.

To observe the formation of core-shell structures in these bimetallic clusters more clearly, we took high-angle annular dark field (HAADF) images of the sample  $Au_1Pd_5$  [Fig. 5(a)]. The difference in the atomic number of Au and Pd produces a strong contrast difference in HAADF images. From Fig. 5(a), we can observe that some particles with bright cores correspond to gold and darker shells correspond to Pd. We can also see that the core size is not homogeneous and changes from particle to particle. Low-magnification

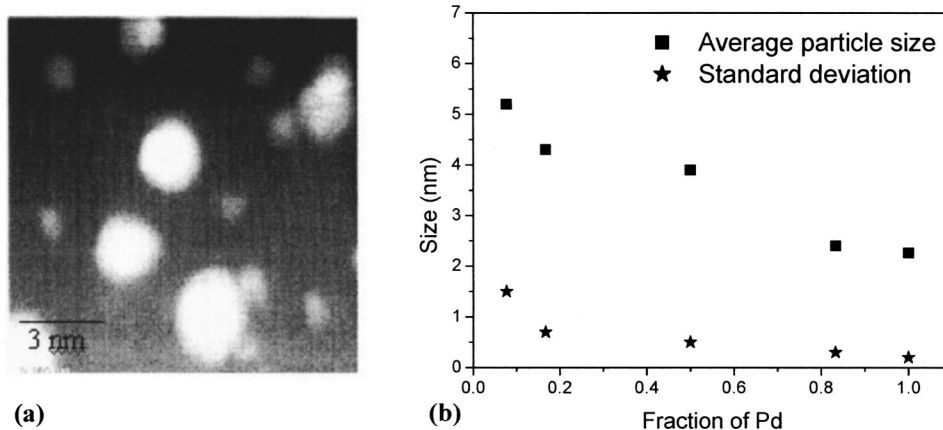


FIG. 5. (a) A typical HAADF image of the  $Au_1Pd_5$  colloidal sample; (b) variation of average particle size and standard deviation in the bimetallic Au-Pd colloids with the variation of Pd content.

TEM images revealed that the average size and size distribution of the bimetallic particles varied with their nominal composition. In Fig. 5(b), the plots of average size and standard deviation (from the Gaussian fits of the size distribution histograms) of the size distributions for the samples prepared with different nominal compositions are presented. We can see that both the average size and standard deviation decrease with the increase of Pd content in the bimetallic particles. X-ray analysis in TEM confirmed the existence of two metals in the particles. Though the exact proportion of the metals varied from particle to particle, the analysis made on a large number of particles agreed well with the nominal composition.

From the experimental results, we can identify the coexistence of several structures such as fcc-like and mtp in the samples prepared with different elemental compositions. In all the cases the internal defects exist, which induce twins even in several fcc-like particles. These internal defects in the clusters are related to the inhomogeneous elemental distribution in them as expected for monometallic or core-shell nanoparticles, where the strain is distributed in the whole structure. Our experimental observations reveal that the core-shell nanoparticles coexist with solid-solution and eutectic configurations, which is supported by our thermodynamical calculations as the differences in their configuration energies are small.

#### IV. CONCLUSIONS

Our simulation and experimental analysis reveal that the structural incoherency dominates the formation of Au-Pd bimetallic clusters, and the stable ordered structures might be the Pd-core/Au-shell, random solid-solution and eutecticlike

structures. Though the Pd-core/Au-shell structure is more favorable, other structures may coexist in the synthesized bimetallic colloids due to the small difference between the configuration energies of different structures. The experimental observations support our theoretical prediction of the coexistence of fcc-like and multiple twinned Au-Pd nano-clusters similar to the case of reported monometallic nano-clusters. We could identify the existence of octahedral and decahedral Au-Pd clusters experimentally. By using energy filtered images, we could identify the existence of Au-core/Pd-shell and Pd-core/Au-shell structures along with other configurations in the synthesized colloidal samples. The Au-core/Pd-shell structure is not stable at high temperatures and can transform into its inverse core/shell structure at about 500 K. These behaviors match with our previously reported results for Au-Cu.<sup>29</sup>

With the help of simulation and experimental methods, we report here on the detailed analysis of atomistic distribution in Au-Pd nanoclusters, including their stability and dynamical behavior. These parameters affect both the structure and the macroscopic properties, particularly the catalytic and electronic ones.

We believe that the different structures, including solid-solution, eutectic-like, Pd-core/Au-shell, and Au-core/Pd-shell ones reported in the literature for Au-Pd samples prepared by similar techniques, is the result of structural incoherency of this bimetallic clusters and common to other bimetallic clusters.

#### ACKNOWLEDGMENTS

We acknowledge J.F. Sanchez Ramirez for his help in preparing Au-Pd colloidal clusters and L. Rendon for technical support in taking HREM images.

\*Author to whom correspondence should be addressed. Electronic address: upal@venus.ifuap.buap.mx

<sup>1</sup>P. Landon, P. J. Collier, A. F. Carley, D. Chadwick, A. J. Papworth, A. Burrows, C. J. Kiely, and G. J. Hutchings, *Phys. Chem. Chem. Phys.* **5**, 1917 (2003).

<sup>2</sup>A. M. Venezia, V. La Parola, V. Nicoli, and G. Deganello, *J. Catal.* **212**, 56 (2002).

<sup>3</sup>A. Benedetti, L. Bertoldo, P. Canton, G. Goerigk, F. Pinna, P. Riello, and S. Polizzi, *Catal. Today* **49**, 485 (1999).

<sup>4</sup>C. Lemire, R. Meyer, S. Shaikhutdinov, and H. J. Freund, *Angew. Chem., Int. Ed. Engl.* **43**, 118 (2004).

<sup>5</sup>A. Enomoto, S. Kurokawa, and A. Sakai, *Phys. Rev. B* **65**, 125410 (2002).

<sup>6</sup>N. T. Tran, D. R. Powell, and L. F. Dahl, *J. Chem. Soc. Dalton Trans.* **2**, 217 (2004).

<sup>7</sup>A. M. Venezia, V. La Parola, G. Deganello, B. Pawelec, and J. L. G. Fierro, *J. Catal.* **215**, 317 (2003).

<sup>8</sup>A. M. Venezia, V. La Parola, V. Nicoli, and G. Deganello, *J. Catal.* **212**, 56 (2002).

<sup>9</sup>Y. H. Chen, Y. H. Tseng, and C. C. Yeh, *J. Mater. Chem.* **12**, 1419 (2002).

<sup>10</sup>G. Cardenas and R. Segura, *Mater. Res. Bull.* **35**, 1369 (2000).

<sup>11</sup>R. Oshima, T. A. Yamamoto, Y. Mizukoshi, Y. Nagata, and Y. Maeda, *Nanostruct. Mater.* **12**, 111, Part A Sp. Iss. SI (1999).

<sup>12</sup>Y. Robach, M. Abel, and L. Porte, *Surf. Sci.* **526**, 248 (2003).

<sup>13</sup>M. C. Gimenez and E. P. M. Leiva, *Langmuir* **19**, 10538 (2003).

<sup>14</sup>H. S. Chang, K. C. Hsieh, T. Martens, and A. Yang, *J. Electron. Mater.* **32**, 1182 (2003).

<sup>15</sup>F. Lehmann, G. Richter, T. Borzenko, V. Hock, G. Schmidt, and L. W. Molenkamp, *Microelectron. Eng.* **65**, 327 (2003).

<sup>16</sup>C. X. Kan, W. P. Cai, C. C. Li, L. D. Zhang, and H. Hofmeister, *J. Phys. D* **36**, 1609 (2003).

<sup>17</sup>M. L. Wu, D. H. Chen, and T. C. Huang, *Langmuir* **17**, 3877 (2001).

<sup>18</sup>N. Toshima, *Pure Appl. Chem.* **72**, 317 (2000).

<sup>19</sup>[http://cyberbuzz.gatech.edu/asm\\_tms/phase\\_diagrams/pd/au\\_pd.jpg](http://cyberbuzz.gatech.edu/asm_tms/phase_diagrams/pd/au_pd.jpg)

<sup>20</sup>R. Hultgren, P. D. Desai, D. T. Hawkins, M. Gleiser, and K. K. Kelley, *Selected Values of Thermodynamics Properties of Binary Alloys* (American Society for Metals, Metals Park, OH, 1973).

<sup>21</sup>J. F. Sanchez Ramirez, G. Diaz, A. Vazquez, and U. Pal, *J. New Mater. Electrochem. Appl.* (to be published).

<sup>22</sup>J. Cai and Y. Y. Ye, *Phys. Rev. B* **54**, 8398 (1996).

<sup>23</sup>A. Banerjee and J. R. Smith, *Phys. Rev. B* **37**, 6632 (1988).

<sup>24</sup>R. A. Johnson, *Phys. Rev. B* **39**, 12 554 (1989).

- <sup>25</sup>J. H. Rose, J. R. Smith, F. Guinea, and J. Ferrante, *Phys. Rev. B* **29**, 2963 (1984).
- <sup>26</sup>J. Riffkin, Center of Simulation, University of Connecticut, USA (2003), <http://ims.uconn.edu/centers/simul>
- <sup>27</sup>H. Takatani, F. Hiori, M. Nakanishi, and R. Oshima, *Mater. Sci. Forum* **445-446**, 192 (2004).
- <sup>28</sup>J. A. Ascencio, C. Gutierrez-Wing, M. E. Espinosa-Pesqueira, M. Marin, S. Tehuacanero, C. Zorrilla and M. Jose-Yacaman, *Surf. Sci.* **396**, 349 (1998).
- <sup>29</sup>J. A. Ascencio, H. B. Liu, U. Pal, A. Medina, and Z. L. Wang, *Microsc. Res. Tech.* (to be published).